BIOLOGY OF REPRODUCTION **84,** 1005–1015 (2011)
Published online before print 3 February 2011.
DOI 10.1095/biolreprod.110.088773

Drosophila Sperm Motility in the Reproductive Tract[1]

Yong Yang and Xiangyi Lu[2]

Institute of Environmental Health Sciences and Department of Biochemistry and Molecular Biology, Wayne State University, Detroit, Michigan

ABSTRACT

Motile cilia and flagella exhibit many waveforms as outputs of dynein activation sequences on the highly conserved axoneme. Motility change of sperm in the reproductive tract is difficult to study and remains an important area of investigation. Sperm typically execute a sinusoidal waveform. Increased viscosity in the medium induces somewhat unusual arc-line and helical waveforms in some sperm. However, whether the latter two waveforms occur in vivo is not known. Using green fluorescence protein imaging, we show that *Drosophila* sperm in the uterus move in circular foci via arc-line waves, predominantly in a tail-leading orientation. From the uterus, a small fraction of the sperm enters the seminal receptacle (SR) in parallel formations. After sperm storage and coincident with fertilization of the egg, the sperm exit the SR via head-leading helical waves. Consistent with the observed bidirectional movements, the sperm show the ability to propagate both base-to-tip and tip-to-base flagellar waves. Numerous studies have shown that sperm motility is regulated by intraflagellar calcium concentrations; in particular, the Pkd2 calcium channel has been shown to affect sperm storage. Our analyses here suggest that Pkd2 is required for the sperm to adopt the correct waveform and movement orientation during SR entry. A working model for the sperm's SR entry movement is proposed.

calcium, female reproductive tract, flagellar motility, Pkd2, primary cilia dyskinesia, sperm, sperm maturation, sperm motility and transport, sperm storage

INTRODUCTION

In species that fertilize internally, sperm travel relatively great distances in the female reproductive tract before reaching the egg. The vast number of sperm in the ejaculate, ranging from thousands to tens of millions, is not sufficient to guarantee successful fertilization [1, 2]. A common theme that has emerged from studies on various organisms is that only a small fraction of inseminated sperm passes through various junctions to enter the uterus or oviduct [3–6]. After that, sperm are generally held in a storage reservoir for hours, days, or even years, depending on the species [7]. In many mammalian species, including *Homo sapiens*, sperm storage involves the binding of sperm to oviductal epithelia at the isthmus [8–10]. This binding is mediated by the interaction of seminal fluid proteins [11–13] on the sperm head with the oviductal receptors [14]. As ovulation approaches, stored sperm are gradually released [15, 16], and concomitantly, their motility is hyperactivated, as exhibited by increased flagellar bend asymmetry and amplitude [17, 18]. The freed sperm move toward the egg in a process likely guided by chemotaxis [19, 20]. An artificial overrelease of sperm at the fertilization site has been shown to increase the incidence of polyspermy [21]. Overall, sperm storage preserves sperm fertility both before and after ovulation and modulates sperm availability, which may have a role in preventing polyspermy.

In *Drosophila*, reproduction involves pronounced sperm storage in specialized organs, the seminal receptacle (SR) and a pair of spermathecae that branch off the main female reproductive tract via separate tubules. The primary storage organ, the SR is an elongated tubule with an extremely narrow lumen through which the sperm enter for storage. Movement of sperm from the relatively unrestricted space of the uterus into the narrow SR tubule likely involves chemotaxis-mediated changes in motility. However, sperm motility is largely uncharacterized in *Drosophila* because of technical difficulty in working with the 1.9-mm-long sperm. The mechanisms by which flagella move have been well characterized. Nevertheless, to our knowledge, flagellar motility has been studied only in cilia and flagella of shorter lengths, ranging from 10 to 200 μm [22–24]. Nearly all flagella, including the fly sperm flagellum, contain a canonical (9+2) microtubule axoneme that extends from the basal body to the distal tip. Flagellar motility is generated by axonemal dynein-driven microtubule sliding that initiates locally but spreads coordinately on the three-dimensional axoneme [23, 25]. The temporal and spatial pattern of dynein activation and inactivation leads to flagellar motility with a characteristic waveform and beat frequency [26–28].

The sperm studied so far typically exhibit sinusoidal waveforms (i.e., bending waves of opposite curvature that alternate in time). The oppositely oriented curvature can be of relatively equal size (symmetrical waves) or unequal size (asymmetrical waves). In the 1960s, Charles Brokaw [29] accidentally discovered two rare waveforms—namely, helical and arc-line waveforms—when some invertebrate sperm were exposed to increased viscosity in the incubation medium. This finding was later extended to sea urchin and quail sperm by Woolley [26, 27], who reported that the sea urchin sperm could execute sinusoidal, arc-line, or helical waveforms interchangeably. This is an interesting finding, because it suggests the potential for new mechanisms by which the (9+2) axoneme is regulated. Based on the current model, the sinusoidal wave is generated by alternating activation and inactivation of two groups of dynein motors, each occupying opposite halves of the axonemal cylinder [30–32], thereby resulting in flagellar bending first to one side and then to the opposite side, in an undulating manner. However, this model does not readily explain the helical waveform, in which the flagellum continuously bends in helical turns. Despite their discovery more than 40

[1]Supported by R01 DK071073 from NIDDK and PKRF Foundation to X.L.
[2]Correspondence: Xiangyi Lu, Institute of Environmental Health Sciences, Wayne State University, Eugene Applebaum, Room 5230.1, 259 Mack Avenue, Detroit, Michigan 48201. FAX: 313 577 0082; e-mail: xlu@wayne.edu

Received: 23 September 2010.
First decision: 4 November 2010.
Accepted: 11 January 2011.

eISSN: 1529-7268 http://www.biolreprod.org
ISSN: 0006-3363

years ago and Brokaw's recent computer modeling of the parameters for the (9+2) axoneme to generate helical bending waves [33], to our knowledge the arc-line and helical waves have not been observed in a normal physiological context of reproduction before the present study. Understanding how the sinusoidal, arc-line, and helical waveforms are interchangeably regulated will provide novel mechanistic insights regarding the regulation of axonemal dyneins, and this would be facilitated in the genetic model system we report here.

Besides waveforms, sperm motility is also regulated by the direction of wave propagation along the longitudinal axis of the axoneme. Most protozoa and spermatozoa start a flagellar wave at the base and propagate it toward the tip. Interestingly, sperm from the Tephritid fly and marine invertebrates *Myzostomum* and *Turritella* can propagate waves in either direction, base-to-tip or tip-to-base, which results in a head-leading or tail-leading movement, respectively [34–36]. If the (9+2) axoneme has an inherent capacity to propagate waves in either longitudinal direction, what determines the direction of a flagellar wave? At this time, the regulation of flagellar wave direction is an unexplored field. In the present study, we used transgenes expressing green fluorescent proteins (GFP) to visualize *Drosophila* sperm head and tail, which otherwise could not be distinguished by morphology. With this technical improvement, we are able to show that the *Drosophila* sperm is a bidirectional swimmer capable of propagating flagellar waves in both axial directions. We also show that they can execute arc-line and helical waveforms. Imaging analyses show that both the waveform and wave propagation direction are under complex regulation during transitory movements between different compartments within the reproductive tract. Furthermore, analyses of loss-of-function *Pkd2* mutant sperm suggest that the Pkd2 calcium channel is required for the sperm to adopt the correct flagellar waveform and wave propagation direction during entrance into the female SR tubule. Overall, the data presented here provide relevant groundwork for future analyses of genes that regulate the arc-line versus the helical waveform, genes that regulate flagellar wave propagation direction, genes that regulate the sperm storage process, and signaling components downstream of PKD2-mediated calcium influx, which is relevant to polycystic kidney disease, left-right body axis determination, and mechano-sensation in a number of physiological processes.

MATERIALS AND METHODS

Drosophila *Genotypes*

Drosophila melanogaster strains were used. *Protamine-GFP* [37] (a second chromosome transgene; obtained from R. Renkawitz-Pohl, Philipps-Universität Marburg, Marburg, Germany) and *Dj-GFP* [38] (a third chromosome transgene; obtained from B.T. Wakimoto, University of Washington, Seattle, WA) were used to visualize sperm head and tail, respectively. Wild-type sperm were obtained from males carrying one copy each of the head and tail GFP reporters. The *Pkd2* mutant alleles, $Pkd2^{KO67}$ [39] and $Pkd2^{1}$ [40], are two complete loss-of-function alleles. To introduce the GFP reporters into the *Pkd2* mutant background, a second chromosome carrying both *Protamine-GFP* and $Pkd2^{KO67}$ was made by chromosomal recombination. A starter stock with the genotype of w^{1118}; *Protamine-GFP* $Pkd2^{KO67}$/*CyO*; *Dj-GFP* was produced. Here, *CyO* is the second chromosome balancer, and it carries the dominant curly wing marker (http://flybase.org/). By crossing this starter stock with the $Pkd2^{KO67}$/*CyO* or $Pkd2^{1}$/*CyO* stock, *Pkd2*-mutant sperm from two allelic combinations, *Protamine-GFP* $Pkd2^{KO67}$/+ $Pkd2^{KO67}$; *Dj-GFP*/+ and *Protamine-GFP* $Pkd2^{KO67}$/+ $Pkd2^{1}$; *Dj-GFP*/+, were generated and analyzed.

Sperm Imaging

Sperm images were captured using a Nikon multizoom AZ100 microscope with a magnification range of 10–320×. The microscope was fitted with a Nikon Intensilight 130W High-Pressure Mercury Lamp; a GFP HC HiSN Zero Shift Filter set with excitation wavelength (450–490 nm), dichroic mirror (495 nm), and emission filter (500–550 nm); and a Photometrics Coolsnap EZ 12-Bit Cooled CCD Monochrome camera. Digital images and video were captured by Nikon NIS-Elements imaging software. To visualize sperm in the female reproductive tract, mating was used to trigger the release of mature sperm from the male seminal vesicle into the ejaculatory duct and, later, into the uterus. The female partners were flies with the $y^{1}w^{1}$ genotype that had normal female fertility. To set up mating, one $y^{1}w^{1}$ female virgin was added to a vial that already contained one male to be analyzed. The female and male flies were aged 2 to 7 days. Mating usually commenced within minutes after adding the female. The starting time of copulation was noted, and the copulating pair of flies was processed at a specific time point depending on the type of sperm movement being studied. For video imaging, relevant tissues were dissected and imaged immediately. For still images, the copulating flies were first fast-frozen in liquid N_2 or dry ice before tissue dissection and imaging. All tissue dissections were carried out in 50% *Drosophila* Ringer Solution at final concentrations of 91 mM KCl, 23 mM NaCl, 1.5 mM $CaCl_2$, and 5 mM Tris-HCl (pH 7.2). Tissues were not fixed, and imaging was done immediately after tissue dissection.

To observe sperm movement inside the uterus, an inseminated uterus was dissected from a mated female within 10–30 min after mating. Sperm are extremely sensitive to mechanical stimulation. Hence, it is important to avoid poking or stretching the uterine wall, because that stops sperm movement inside the uterus. To release sperm from the uterus into the buffer, a thin needle was used to quickly puncture the uterine wall. The sperm released in this manner were free only at one end (either proximal or distal end), whereas the other end was anchored to the uterine wall. However, wave propagation was easily observable at the free ends of these sperm. Individual sperm without contact with the uterine wall or other sperm, as shown in Figure 1C, could only be obtained fortuitously.

To capture stalled sperm tails within the lumen of the proximal SR (PSR) (see Supplemental Movie 6; all Supplemental Data are available online at www.biolreprod.org), mating was terminated 7 min after onset, before the mating pair was separated. At this time, the sperm had just entered the uterus, but no sperm had moved all the way into the final sperm storage site, the distal SR (DSR). When the female reproductive tract was removed and placed in the dissection buffer at such an early time after mating, the progressive movement of sperm tails was found to stall within the PSR, and no sperm moved into the DSR. It is not known why the movement stalled, but perhaps the SR entry signal was insufficiently produced when the uterus was taken out of the female too soon after mating. In contrast, when the uterus was dissected at 15–45 min after mating, sperm were able to move from the uterus through the PSR into the DSR (see Supplemental Movies 7 and 8). These findings suggest that at early time points of sperm storage, the PSR entry signal might not be fully established, which could make the sperm more sensitive to the mechanical perturbation of dissection. Beyond 1 h after mating, the entry signal might be diminishing, and there could be a competing signal that stops sperm storage because the PSR lumen remains vacant at the end of sperm storage. For these reasons, we focused on the time period from 15 to 45 min after mating, which was a highly reproducible period for observing sperm passage through the PSR, as shown in Supplemental Movie 8.

Other experimental procedural concerns are as follows: 1) The PSR can be slightly uncoiled manually without affecting sperm entry into the DSR. However, sperm movement into a completely straightened PSR was not observed. It is possible that the curvature of the coiled PSR tubule exerts some sort of mechanical loading that drives the movement of passing sperm. 2) It is important to locate the division point between the PSR and DSR, because sperm movement is different in these two compartments. As shown in Supplemental Movie 7, the PSR tubule forms a convoluted, circular fold that usually has a spatial overlap with the folded DSR tubule. This spatial overlap could give the illusion that some sperm move out of and then go back into the DSR, especially if you start a video recording when some sperm are moving through the circular PSR loop that lies partially underneath the DSR. 3) Because sperm are naturally sensitive to mechanical stimulation, one should avoid stretching and poking the tissues while unfolding the PSR for imaging, because mechanical perturbation can cause the sperm to stop, retract, or exhibit other unpredictable behavior. For this reason, still images were obtained from fast-frozen flies to confirm the observations from live imaging. 4) It is better to leave the ovary attached to the oviduct, because this prevents possible flooding of the internal environment by the dissecting buffer.

To observe sperm in the uterus enter the PSR, as shown in Supplemental Movie 9, the uterus was dissected 15 min after mating onset and mounted on the slide with the dorsal surface of the uterus facing down. The video was captured using an inverted microscope with a 40× objective, focusing right underneath the dorsal surface of the uterus, which is on the side opposite that of the PSR opening on the ventral oviduct wall. To obtain still images of sperm passing through the PSR, the copulating flies were fast-frozen on dry ice before

tissue processing. The PSR was uncoiled and straightened manually by forceps before imaging. We quantified the orientation of sperm entry (head first vs. tail first) from well-isolated individual sperm that entered the PSR at 15 min after mating onset. To be counted as a leading structure, the head or tail had to move at least 0.1 mm into the PSR. To be counted as a tangled sperm, the sperm had to be folded at least once. To observe sperm exit the DSR, the mated females were allowed to lay eggs for 24 h after mating. Many eggs laid by the mated females during the first 24 h were fertilized; thus, the 24-h time point was appropriate for observing the exit movement of sperm.

To observe sperm movement inside the DSR, the uterus from a mated female was mounted on a slide. Without further manipulation, the DSR is already exposed and ready for imaging, whereas the PSR is hidden under the DSR. For wild-type flies, the large number of sperm stored prohibited a clear observation of sperm movement. To overcome this, we successively mated one male with multiple females to reduce the number of sperm in the DSR. To release stored sperm from the DSR, the mated females were allowed to live for 11 days in the absence of additional males. The uterus was then dissected and the PSR partially uncoiled to allow a cut in the middle of the tubule. Stored sperm exited the cut opening into the buffer by themselves.

RESULTS

Sperm in the Uterus Move in Circular Foci via an Arc-line Waveform

To observe flagellar orientation in the reproductive tract, sperm head and tail were marked with *Protamine-GFP* [37] and *Dj-GFP* [38], respectively, and movement was observed by fluorescence microscopy. In the uterus, *Drosophila* sperm move in circular foci (Fig. 1A and Supplemental Movie 1) by propagating circular flagellar bends (Fig. 1B and Supplemental Movie 2) that resemble the meander or arc-line waveform exhibited by sea urchin and quail sperm [26, 27]. The features of the arc-line waveform of *Drosophila* sperm is shown with a sperm from the uterus (Fig. 1, C–G, and Supplemental Movie 3). A single fly flagellum can form up to 10 arc-line bends that stack in a figure-8 configuration (Fig. 1C). Each arc-line bend is formed by propagating an open arc that then closes. All new arc-line bends (highlighted outlines in Fig. 1, D–G) originate from the tail end, repeatedly, at approximately 0.13 mm from the tip. The thrust direction of each new arc-line bend alternates in bipolar directions, thus producing a folded flagellum in a figure-8 shape. Nineteen-and-a-half bends were produced in 41.9 sec, giving rise to an average speed of one bend per 2.15 sec. For sinusoidal waves, the undulating bends typically spread apart into a linear array. In contrast, the bends of the observed arc-line waves are compressed such that the bends lie on top of one another. Nevertheless, the new bend and all intervening bends propagate from the tail end toward the head end, producing a true velocity (64.5 μm/sec) as defined by the speed of the head being dragged along the figure-8 path. The bend-stacking pattern of the quail sperm is slightly different [27].

Sperm Are Capable of Base-to-Tip or Tip-to-Base Waves

Because it is difficult to analyze sperm movement in the crowded sperm mass in the uterus, sperm were released from the uterus by needle puncture. In most cases, released sperm were free at only one end, with the remaining flagellum anchored by the uterine wall. Interestingly, such released sperm propagated tip-to-base waves when distal sperm flagellum was anchored (Fig. 1H and Supplemental Movie 4) or base-to-tip waves when proximal flagellum was anchored (Fig. 1I and Supplemental Movie 5). The tip-to-base or base-to-tip waves observed under these conditions were stable and did not reverse. Correlation of the wave direction with the flagellar anchorage location was strict, and no difference was found between the wild-type and the *Pkd2*-mutant sperm ($Pkd2^{ko67/ko67}$, n > 30 each).

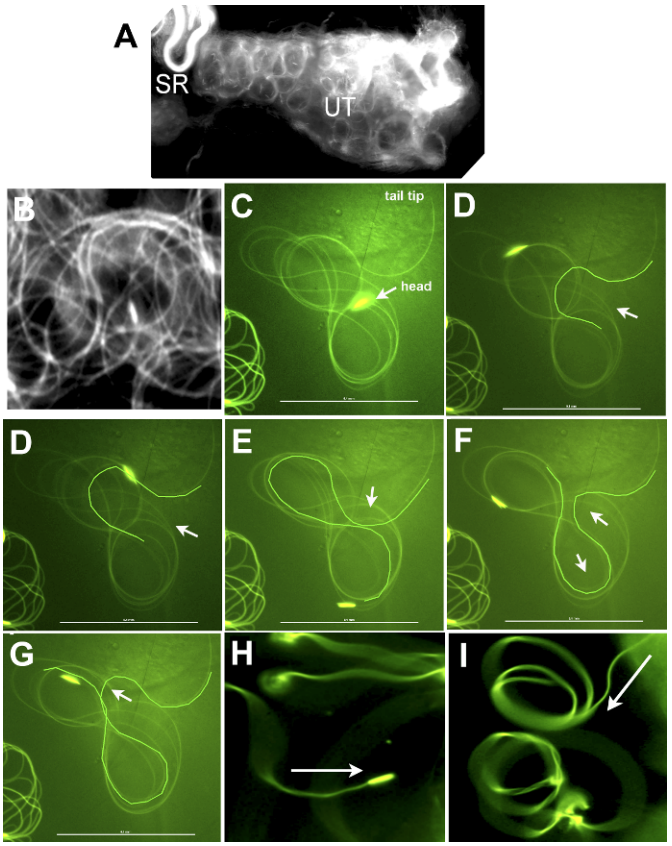

FIG. 1. The arc-line, base-to-tip, and tip-to-base waves of sperm from the uterus. Snap views of live samples are shown. **A**) The moving sperm (~5000 sperm) appear as circular foci in the uterus. **B**) A close-up view of the sperm in **A** shows circularly bent flagella (Supplemental Movies 1 and 2). **C**–**G**) A sperm released from the uterus executes an arc-line waveform (Supplemental Movie 3). **C**) A single fly flagellum forms up to 10 arc-line bends that stack into a figure-8 configuration. **D**–**G**) Sequential snap views showing formation of new arc-line bends (highlighted). Similar to sinusoidal waves, all new bends initiate at one of the flagellar ends (the tail end in this case). The arrow points to the thrust direction of a new bend that protrudes out as an open arc that then closes. The thrust direction alternates in opposite directions. The arc-line bends propagate through the entire folded flagellum, as evidenced by the moving head as it is continuously dragged behind its flagellum on the figure-8 path. **H**) Tip-to-base waves are observed when the distal flagellum is anchored (Supplemental Movie 4). **I**) Base-to-tip waves are observed when the proximal flagellum is anchored (Supplemental Movie 5). Arrows in **H** and **I** point to the direction of wave propagation. Bar = 0.1 mm.

The anchorage-dependent wave propagation direction may be induced as an obstacle avoidance response. For example, trypanosomes propagate tip-to-base waves for general movement but transiently reverse to base-to-tip waves for backing up in response to obstacles [41, 42]. Alternatively, the anchorage-dependent wave direction could be a flagellar response to a newly introduced restraining site following anchorage of the distal or proximal flagellum. The current flagellar propulsion theories [23], including the Geometric Clutch model [43], predict that flagellar bend propagation requires a fixed site that restricts the sliding of doublet microtubules. The site that naturally restrains microtubule sliding is usually at the base of the head. Manipulations such as mechanical bending, laser-induced flagellar fusion, or protein cross-linking have been used to introduce new restraining sites in the middle of several

flagellar types [44–49]. Waves were found to propagate from the manipulated sites, and the original wave polarity of the parent flagellum was maintained [44–49]. For sea urchin or bull sperm that normally execute only base-to-tip waves, no manipulation has been found to induce tip-to-base waves [44–48]. For trypanosomes, which are capable of bidirectional waves, waves were found to propagate in both directions after laser fusion created a new restraining site [49]. To our knowledge, possible effects of restraining sites on long flagella have not been determined. The fly sperm flagellum does contain a conserved (9+2) axonemal structure, although it also has nine accessory singlet microtubules surrounding the (9+2) core. Our observation of anchorage-dependent tip-to-base or base-to-tip waves suggests that the *Drosophila* sperm flagellum can propagate waves in both axial directions, and this is further demonstrated below.

Sperm Enter the SR Tubule Predominantly with Tail-leading, Parallel Formations

From the uterus, sperm enter the SR tubule that branches off the oviduct wall near its junction to the uterus (see Fig. 3D). The SR tubule is a 2.2-mm-long, dead-end tubule that is just slightly longer than the sperm. However, the SR lumen is extremely narrow. The PSR (~19 μm wide) (manually straightened part in Fig. 2, A–D) serves as the passageway to the slightly enlarged DSR (~24 μm wide) (folded part in Fig. 2, B–E). The DSR serves as the reservoir for storing sperm in folded form (Fig. 2E). To capture still images of sperm passing through the PSR, virgin females without sperm stored from a previous mating were mated with males, and the copulating flies were fast-frozen before obtaining PSR for imaging. The still images thus obtained showed parallel formations of sperm flagella consisting of multiple intertwined tails that enter the PSR as a bundle (Figs. 2, A–C, and 4B). The parallel formation is in clear contrast to the folded flagella in the uterus (Fig. 1B), suggesting that PSR entry involves a waveform transformation from the circular to the extended linear form. To determine initial sperm orientation, still images were obtained from copulating flies fast-frozen 15 min after mating onset. This early time of sperm storage provided a quantification of initial sperm entry orientations into the PSR. Results showed that the tail-leading orientation occurred at a frequency of 80% (20/25 sperm) (Fig. 2, A and B), whereas the head-leading orientation (2/25 sperm) and flagella with one hairpin-shaped fold (3/25 sperm) (similar to that shown in Fig. 6D) were found in only a minority sperm. The latter two types of atypical sperm orientations were found in the mix of parallel flagellar bundles that entered the PSR (Fig. 2A; see also Fig. 4B).

Dynamic Aspect of the Sperm SR Entry Movement

To understand the dynamic process of sperm entry, uteri were dissected from the females before the mating pairs were separated (~7 min after copulation onset). This time point is soon after sperm enter the uterus, but the sperm have not yet moved into the DSR. When the uterus was dissected from the female at this time, one sperm bundle consisting of multiple tails was found to have stalled within the PSR lumen (Fig. 3A and Supplemental Movie 6). These tails made waving movements but did not progress into the tubule. All sperm in the stalled bundle were in a tail-leading orientation, and a head-leading orientation or flagellar loop was not found ($n > 8$). Possible reasons for the stalled movement include chemical or mechanical disturbances or insufficient production of PSR-entry signal at the early time of dissection. In contrast, when the uterus was dissected from the female at later times (15–45 min after mating), we observed that sperm were moving from the uterus through the PSR and into the DSR without a change of movement direction (Supplemental Movies 7 and 8). While incoming sperm still passed through the PSR to enter the DSR, those sperm that had already entered the DSR showed restricted movement within the DSR (Supplemental Movie 8).

If a group of sperm moves into the PSR with tails leading, lagging heads are expected to form clusters. Indeed, we observed the formation of head clusters (defined as two or more heads with a separation of less than one head-length) in the uterus (Fig. 3F) and in the PSR (Fig. 4, C and D). Supplemental Movie 9 captured a head cluster as it was rapidly (~0.4 sec) formed from one of the circular sperm foci in the uterus (Fig. 3F and Supplemental Movie 9). The head cluster moved upward toward the PSR opening (Fig. 3D) on a visible line of GFP fluorescence (referred to as GFP trail) because of GFP associated with the flagella (Fig. 3E). In this experiment, an individual sperm head appeared as a short green stick, whereas an individual flagellum was too weak to see. Two sperm heads were moving ahead of the head cluster, and 10 sperm heads were following behind it on the GFP trail. Because these sperm heads (except the atypical head discussed below) moved upward on the GFP trail in a straight trajectory (without turning), the GFP trail is likely formed by sperm moving in parallel to one another in formations similar to the captured tail bundles in the PSR (Figs. 2A, 3A, and 4B). In addition, the spacing between two adjacent sperm heads on the GFP trail is approximately 70–320 μm, which is much shorter than the full-length sperm of 2 mm, suggesting that sperm moving on the trail are likely overlapping along their lengths. We also determined sperm head spacing at a late (~45 min after mating) and perhaps slower phase of sperm storage by examining sperm passing through the PSR on video recordings. Overlapping sperm arrays consisting of at least five to eight sperm with head spacing ranging from 0 to 1.5 mm were observed to enter the DSR without making turns (Supplemental Movies 7 and 8 and Supplemental Table S1). Thus, it appears that the *Drosophila* sperm generally move through the PSR in overlapping, parallel arrangements. Such movement of sperm in groups could be viewed as a form of sperm cooperation. Various different forms of sperm cooperation have been shown in European wood mice [50] and many other species, with reproductive advantages demonstrated in many cases [51].

Another interesting observation from Supplemental Movie 9 was that as the head cluster was forming, it appeared to have incorporated an atypical sperm (red arrowhead in Fig. 3F). The head of the atypical sperm, initially together with the head cluster, could be recognized by its separation from the head cluster and movement in the opposite direction of the head cluster (Fig. 3F). The atypical sperm head then underwent a rapid U-turn (Fig. 3H) before resuming upward movement toward the PSR opening (Fig. 3I). Later, we describe a model to explain the motility behavior of the majority of sperm during PSR entry as well as the unusual behavior of a minority of atypical sperm (see *Discussion*).

Movement of Sperm Inside the DSR Storage Site

The DSR is only half the length of sperm. Sperm inside the DSR are folded as shown in Figures 2E (still image) and 5A (video snap view). The folded form is derived from hairpin-shaped flagellar bends that the sperm propagates inside the DSR (Supplemental Movie 10). The speed of bend propagation can be inferred from the speed of the moving head, which is mostly dragged behind the flagellum while the flagellum

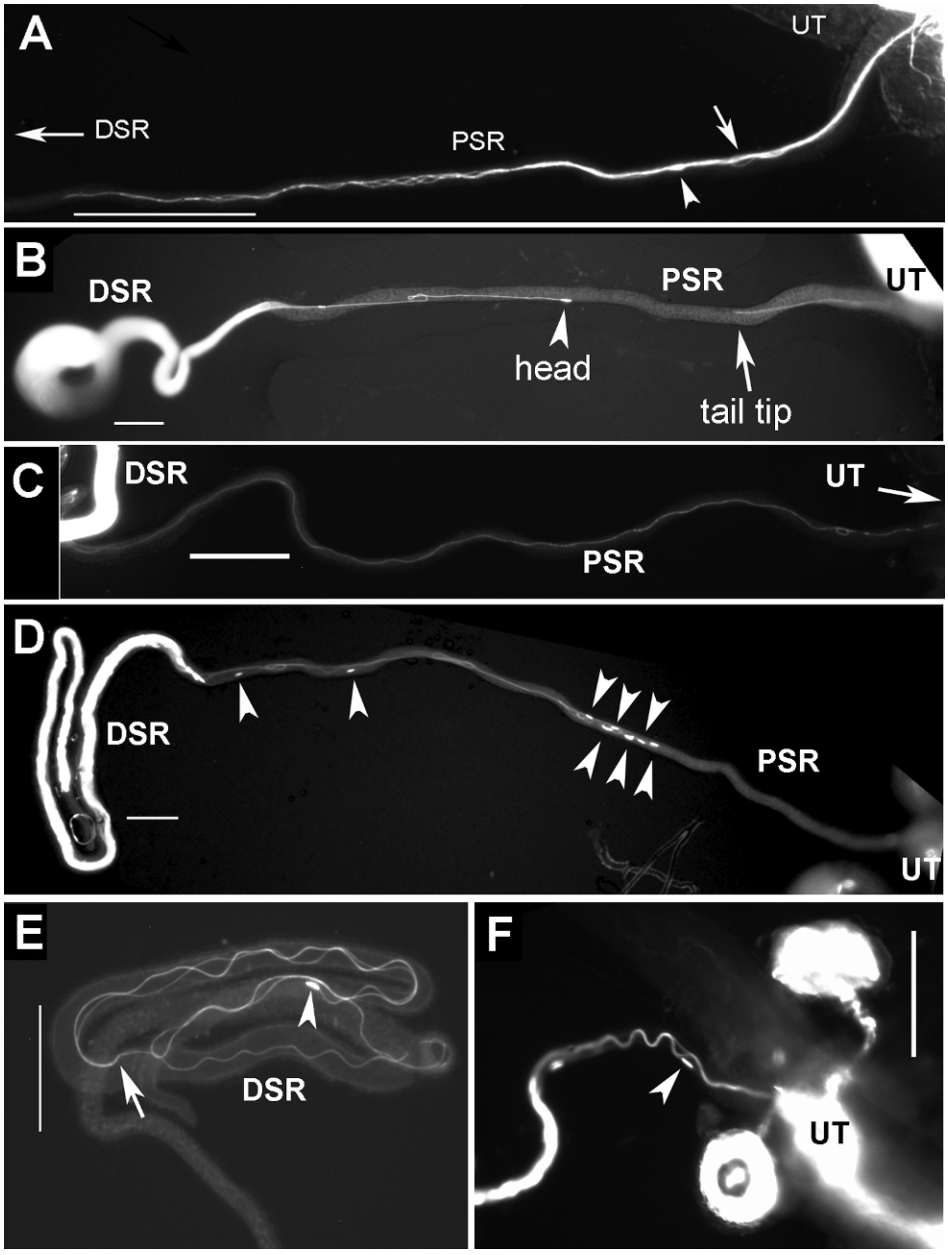

FIG. 2. Parallel formation of flagella during SR entry and exit. Still images from frozen samples are shown. **A–C**) Images of sperm entry movement were obtained 15 min to 1 h after mating. **A**) Sperm entered the PSR in a parallel formation consisting of multiple sperm tails twisting around each other like a bundle. This tail bundle has entered halfway (0.5 mm) into the PSR. One head (arrowhead) and one flagellar loop (arrow), representing sperm with atypical flagellar configurations, were found in the mix of the tail bundle in **A** (Fig. 3F and Supplemental Movie 9). An explanation for these atypical sperm is given in Figure 8. **B**) Two sperm exhibit tail-leading PSR entry movement: One just entered the PSR, and the other nearly entered the DSR. The flagella of these sperm were in extended linear shape (a small fold was caused by unfolding the naturally folded PSR). **C**) Sperm moved across the PSR lumen without flagellar folds. **D** and **F**) Images of sperm exit movement were obtained 24 h after mating, and sperm exhibited head-leading movement (arrowheads indicate sperm heads). **E**) A sperm inside in the DSR is folded (arrow indicates, tail tip). Bar = 0.1 mm.

slithers through its folded form. In a recent study [52], the sperm head was labeled with GFP, but the flagellum was not. In that case, the sperm head appeared to make rapid, 180° flip-flop turns in the DSR. As shown in Supplemental Movie 10, the turning movement of the sperm head is generated when the head is dragged through a U-shaped region of the folded flagellum. The direction of the head movement generally stays the same with respect to its flagellum. Occasionally, the head pauses and then briefly reverses to a head-leading movement before being dragged backward again by its flagellum; this movement sequence appears as a to-and-fro, bidirectional movement in the DSR.

Sperm Released from the Storage Site Propagate in Head-leading Helical Waves

During the weeks of extended storage, a small number of sperm gradually exit the DSR to fertilize the eggs [53]. We determined the orientation of returning sperm by fast-freezing the mated females 24 h after initial mating. Sperm inside the PSR at this time are those that have returned from the DSR, because mated flies start to lay fertilized eggs 5–6 h after mating and unstored sperm have been mostly ejected from the uterus by the fifth hour after mating [54]. To travel out of the PSR, sperm assume an extended linear form, but this time with a head-leading orientation (100%, 30/30 cases) (Fig. 4D).

To show that sperm undergo an orientation switch from tail-leading to head-leading movement after residing in the DSR, sperm were released from the DSR into dissection buffer on a microscope slide. After 11 days of DSR residence, the released sperm, which were free of anchorage at both ends, moved with the head leading (Fig. 5B and Supplemental Movie 11). Essentially all sperm released in this manner executed head-leading, clockwise rotations on left-handed helical paths ($n > 50$). The buffer and surface conditions on the glass slide likely are substantially different from conditions in the PSR lumen. Under that experimental condition, which did not provide any spatial restriction, the diameter of the helix varied from 0.06 to 0.15 mm. Similar to the helical waveform of sea urchin sperm

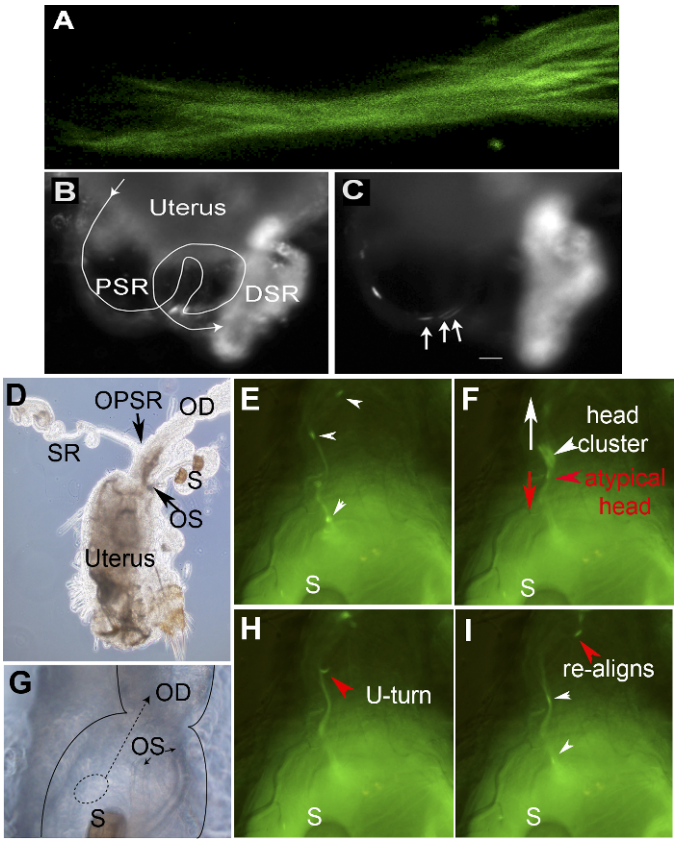

FIG. 3. Leading tails and lagging heads. The dynamic process of PSR entry is shown here with video snap views of live samples. **A**) Multiple sperm tails enter the PSR in parallel formation like a bundle; the sperm are labeled with both head and tail GFP (Supplemental Movie 6). **B** and **C**) The sperm (labeled with head GFP only) pass through the convoluted PSR tubule (line trace in **B**) and enter the folded DSR on the right, which already contained a lot of sperm, as indicated by the bright fluorescence (Supplemental Movies 7 and 8). Arrows in **C** point to a cluster of three sperm heads that moved in one overlapping array consisting of eight sperm, which was then followed by a second array consisting of five sperm. The array is defined by having head-to-head spacing shorter than one sperm length of 2 mm (Supplemental Table S1). All of these sperm went through the PSR without to-and-fro motion and without turning or changing of the direction of movement. The time was 45 min after mating. **D**) Image of the uterus shows the relative locations of the oviduct (OD), ventral SR, and dorsal spermathecae (S). Arrows point to the openings of SR and spermathecae (OPSR and OS, respectively). **G**) Image at the uterus-oviduct junction provides spatial orientation for Supplemental Movie 9 (**E**, **F**, **H**, and **I**). Notice that the spermathecae are folded back onto the dorsal surface of the uterus. The dashed circle represents the location of the sperm focus, from which sperm initiate PSR entry movement in Supplemental Movie 9. The dashed arrow points to the direction of moving parallel sperm array. **E**, **F**, **H**, and **I**) Sequential snap views from Supplemental Movie 9 (time index, 1.375, 1.750, 3.375, and 4.375 sec). When multiple sperm flagella align into a parallel bundle, this appears as a GFP trail that leads upward toward the OPSR. **E**) Two sperm heads are on the GFP trail, and a head cluster is just about to be pulled out of the circular sperm focus in the uterus. **F**) The head cluster is pulled out and moving upward on the GFP trail. The head cluster contained one atypical sperm (red arrowhead), which is identifiable from its opposite moving direction and separation from the head cluster. The white arrow points to the upward-moving direction of most sperm, whereas the red arrow points to the downward-moving direction of the atypical sperm. **H** and **I**) The atypical sperm head undergoes a U-turn (**H**), and it rejoins the majority of sperm on the GFP trail (**I**). Original magnifications ×400 (**A**), ×20 (**B**, **C**), ×10 (**D**), ×40 (**E**–**I**).

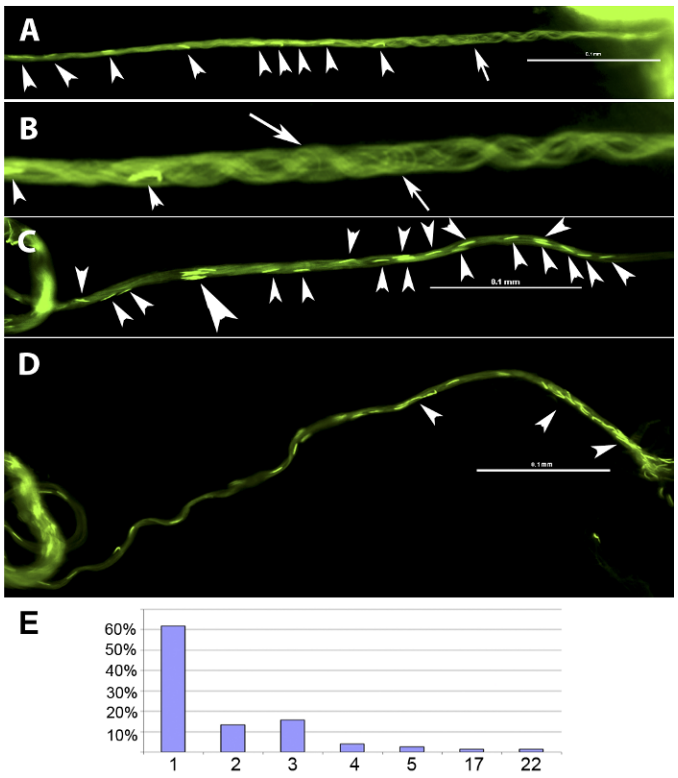

FIG. 4. Arrangement of sperm bundle inside the PSR. **A**–**D**) Still images of fast-frozen, wild-type sperm that entered the PSR. The uterus is positioned on the right beyond the view, and the DSR is on the left. **A**) This PSR is filled with sperm, with heads visible along the length (arrowheads). **B**) An enlarged image of **A** shows intertwining sperm flagellar bundles that are mostly parallel to each other. A small number of bent flagellar loops (arrows) are present in the mix. **C**) The sperm heads in the bundle are either well separated or clustered with a separation spacing of less than one head length (big arrowhead). **D**) Some clusters (arrowheads) contain as many as 22 sperm. **E**) The number of heads found in a cluster (x-axis) and observed frequency (y-axis) are plotted (n = 164 heads). Bar = 0.1 mm.

in a high-viscosity environment [26], the helical movement of the fly sperm is associated with low-amplitude, vibrating waves that make the flagellum appear to be thicker than it actually is (Fig. 5B). Brokaw's recent computer modeling indicated that internal rotation or writhe of the axoneme can generate helical waveforms via local curvature control of dynein motor activity [33]. This provides a mechanism for generating helical waves without involving the typical sinusoidal waves [33]. In addition, two or three helical modules separated by link regions were seen to form for a single flagellum. While these modules are turning semi-independently of each other because of differential torsion at the link regions, overall movement as a whole is smooth and coordinated (Supplemental Movie 11). The flagellum of the African trypanosome was recently shown to form two helical modules separated by kinks [55].

Pkd2 *Is Required for Sperm Entry Movement into the PSR*

A loss-of-function *Pkd2* mutation impairs male fertility; however, gross sperm motility, such as beat frequency, was unaffected in mutant sperm that were removed from the male seminal vesicle and analyzed in vitro [40]. Transfer of the mutant sperm from the male to the female uterus was also unaffected [39, 40]. As mentioned earlier, partially anchored *Pkd2*-mutant sperm could propagate base-to-tip or tip-to-base waves ($Pkd2^{KO67/KO67}$, n > 30 each), with no obvious

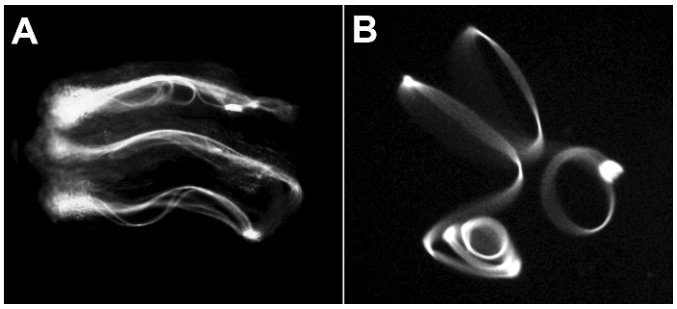

FIG. 5. Sperm movement during and after storage in the DSR. Video snap views of live samples are shown. **A**) Several sperm move in folded forms in the DSR by protruding, hairpin-shaped flagellar bends (Supplemental Movie 10). The head is dragged backward by its flagellum as the flagellum slithers through its folded form. Occasionally, the head pauses and reverses to head-leading movement for a brief moment, resulting in a to-and-fro pattern of movement. **B**) This sperm released from the DSR is executing a helical waveform with head-leading clockwise rotations (Supplemental Movie 11). The sperm is free floating and not anchored at any points on the slide. Original magnification ×20.

differences compared to wild-type sperm. However, parallel mutant sperm bundles similar to wild-type sperm shown in Figure 4 were not found in the PSR lumen (n ~ 300) by video or still-image analyses under the same experimental conditions used for the wild-type sperm. This finding is consistent with the extreme phenotype of *Pkd2*. Wild-type males consistently result in storage of 275–404 sperm in the female DSR (n = 18), whereas the $Pkd2^{KO67/KO67}$-mutant males lead to an average of 2.8 sperm in the female DSR, which corresponds to 1% of the normal sperm storage level (n ~ 400).

To determine the motility defects of the mutant sperm, we examined initial sperm entry into the PSR from still images of individual sperm obtained 15 min after mating onset as was done for the wild-type sperm. Two independently isolated, strong loss-of-function alleles, $Pkd2^{KO67}$ [39] and $Pkd2^{1}$ [40], were analyzed. A consensus observation was that the mutant sperm showed increased head-leading orientation and excessive flagellar folding. Because of increased head-leading orientation, multiple head-leading mutant sperm were found to enter the PSR at the same time (Fig. 6A), whereas for the wild-type sperm, only single (not multiple) head-leading sperm were observed, and at a low frequency. For quantitative comparison, 80% of wild-type sperm at PSR entry were tail leading, 8% were head leading, and 12% had folded flagella (n = 25). In contrast, for $Pkd2^{KO67/1}$ sperm, 15% were tail leading, 30% were head leading, and 55% had folded flagella (n = 84), and for the $Pkd2^{KO67/KO67}$ sperm, 14.9% were tail leading, 46.5% were head leading, and 38.6% had folded flagella (n = 101). These initial deviations from the normal pattern of flagellar configuration at 15 min after mating onset reflect the underlying motility defect of the mutant sperm. Further movement with the abnormal motility resulted in more severe phenotypes at later time points (1–4 h after mating) in that essentially all mutant sperm in the PSR had folded flagella. Folded flagella were found in freshly dissected PSR at later time points when sperm storage had stopped, as indicated by the extrusion of inseminated sperm out of the uterus, suggesting that the folded flagella were trapped in the PSR and unable to move into the DSR (n = 59). These folded mutant sperm exhibited different degrees of folding, from the weakest with the head slightly folded (Fig. 6B) to multiple folds in figure-8 shapes that resemble the folded sperm from the uterus (Fig. 6, E and F) to multiple buckles along the

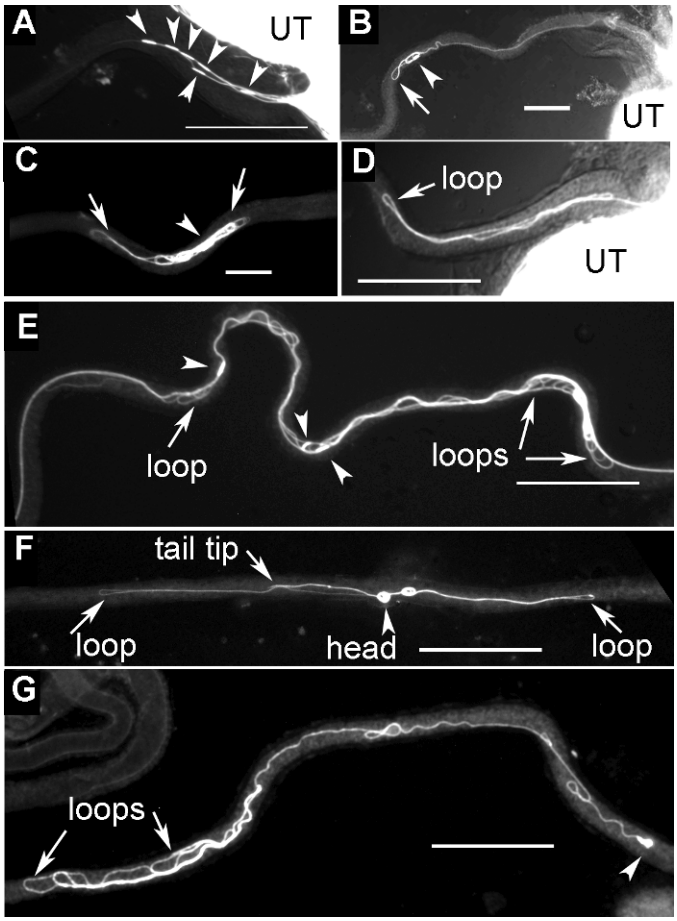

FIG. 6. Abnormal configurations of *Pkd2* mutant sperm during PSR entry. Still images from frozen samples are shown. These are representative images of *Pkd2*-mutant sperm that moved into the PSR but appeared to be trapped. The uteri are positioned to the right. **A**–**D** and **E**–**G** show sperm from $Pkd2^{KO67}/Pkd2^{KO67}$ and $Pkd2^{1}/Pkd2^{KO67}$ males, respectively. **A**) Six sperm moved into the PSR with head-leading (arrowheads) instead of tail-leading orientation observed for most wild-type sperm. **B**) The head of the sperm was leading, but flagellar loops (arrow) began to form. **C**) A sperm was folded excessively into an abnormal yarn ball appearance. **D**) A hairpin-shaped flagellar loop entered the PSR (Supplemental Movie 12). **E**) Several sperm were tangled together and contained multiple figure-8-shaped loops (arrows). **F**) A figure-8-shaped flagellum was located within PSR lumen. **G**) A tail-leading sperm was found to form multiple flagellar buckles. Bar = 0.1 mm.

flagellar length (Fig. 6G) and excessively folded flagellum in the form of a yarn ball (Fig. 6C).

A folded mutant flagellum might be generated when the sperm has made multiple turns or moved with an abnormal waveform. To distinguish these possibilities, we examined the formation of a folded sperm in the PSR by video. The video (Supplemental Movie 12) showed that a $Pkd2^{KO67/KO67}$ mutant sperm (arrowhead points to the sperm head) propagated two hairpin-shaped flagellar bends into the PSR lumen (labeled 1 and 2 in Fig. 7), whereas the head stayed in the general vicinity of the uterus-PSR junction, indicating that this folded flagellum was not formed because the sperm had made multiple turns. Later, the folded sperm was stuck in the PSR lumen and could not break free even though the flagellum continued to beat (Supplemental Movie 12). The protrusion of hairpin-shaped flagellar bends may indicate an inappropriate occurrence of the arc-line waveform in the PSR lumen. Some figure-8-shaped

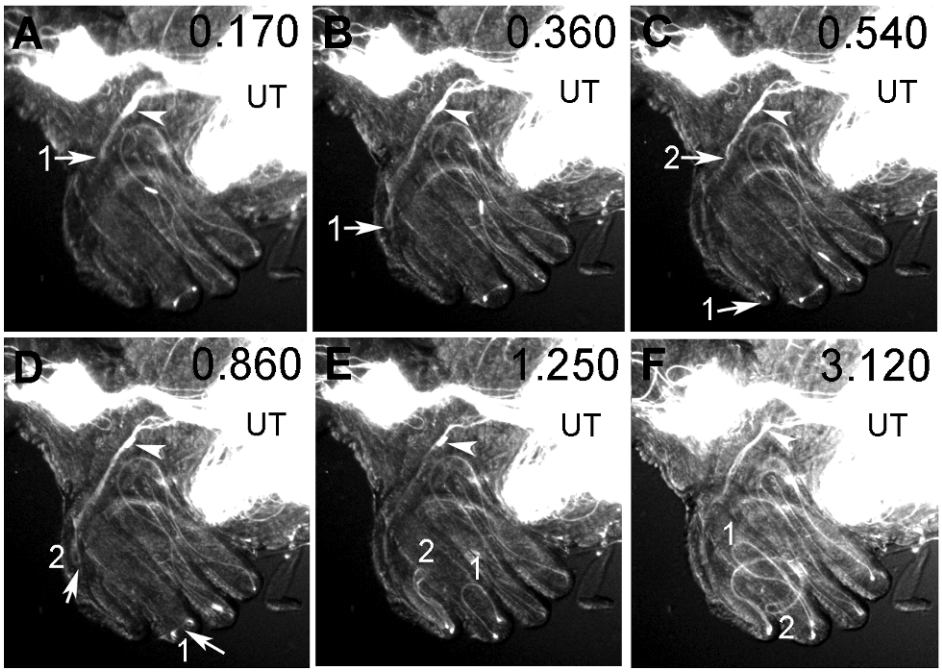

FIG. 7. Abnormal propulsion of *Pkd2*-mutant flagellum during PSR entry. Sequential video snap views from Supplemental Movie 12 are used to show the abnormal propulsion of the mutant sperm at the uterus-PSR junction (**A**–**F**). To orient viewers, the PSR tubule forms the left outer rim of the coiled SR complex, going underneath the DSR tubules that face the reader. The sperm head (arrowhead) stayed in the general vicinity while its flagellum was protruding two hairpin-shaped flagellar loops (labeled 1 and 2) into the PSR lumen. The "hairpins" soon became stuck even though the flagellum continued to beat. The head was pulled along but stayed in the general area. The time index (sec) is shown at top right corner of each frame. Original magnification ×20.

Pkd2-mutant sperm in the PSR resemble the figure-8-shaped sperm from the uterus (Fig. 6F).

DISCUSSION

The present study reports diverse motility changes of *Drosophila* sperm in the female reproductive tract. We discuss the possible relevance of the observed sperm motility with respect to reproductive fitness of this organism. Many of the speculations below are rudimentary; however, they are generally consistent with the fundamental principle that reproductive success depends on efficient interaction between sperm and the female reproductive tract. Optimization of this interaction to achieve maximum fecundity has been the driving force for the coevolution of sperm and the female reproductive tract [56, 57]. For example, the length of the female SR correlates closely with sperm length in many insects and in a dozen *Drosophila* species [58–60]. In the laboratory, selection for increased SR length results in rapid and significant increases in sperm length in as few as 37–42 generations [61]. Second, the stored sperm in the female's DSR are rapidly displaced by incoming sperm from a second male [52]. This results in more progeny fathered by the second male than by the first male, which is referred to as sperm competition. In *Drosophila*, success of sperm of a particular length in sperm competition was found to depend on the length of the female's SR [61]. Long sperm have advantages over short sperm in sperm competition, but this is true only in the context of a long female SR (a short SR does not discriminate against short or long sperm) [59, 61]. Understanding *Drosophila* sperm motility may lead to a better understanding of sperm competition and the coevolution of sperm and the female reproductive tract [58, 62].

Regulation of Waveforms

The *Drosophila* sperm is capable of at least two alternative waveforms, the arc-line and helical waveforms. The arc-line waveform has many features of the regular sinusoidal waveform, except that each consecutive bend stacks on top of the previous one instead of spreading out into a linear array. Spatial compression of the bends plus alternating bipolar bend-thrusts lead to folding of the flagellum into a figure-8 shape. Nevertheless, the arc-line bend propagates through the entire flagellum, as evidenced by the moving head, which has a true velocity on the figure-8 path. A single fly flagellum forms 10 arc-line bends that stack into a compact moving entity, which allows movement while reducing the risk of interflagellar crossing over and entanglement. This could be an important adaptation for long sperm, because the occurrence of the compact arc-line waveform in the uterus coincides with the capacity of the uterus to accommodate 3000–5000 sperm after a single insemination. In the DSR, the sperm move by propagating hairpin-shaped flagellar bends, which may be a variation of the arc-line waveform within the spatial restriction of the DSR lumen. Similar to sperm in the uterus, the head of sperm in the DSR is predominantly dragged by its flagellum while the flagellum slithers through hairpin-shaped bends. Bend propagation can be inferred from the speed of the moving head as it is being dragged along the folded flagellar path. Furthermore, the movement of *Drosophila* sperm is semistationary in the uterus and the DSR. The alternating bipolar bend-thrusts of the arc-line waves appear to be instrumental for generating the semistationary movement.

In contrast to the arc-line waveform, the helical waveform is well suited for rapidly advancing movement on a straight trajectory [26]. The imaging data suggest that the sperm flagella predominantly form overlapping parallel arrays during PSR entry, although a small number of bent flagellar loops was observed among the parallel flagellar bundles (Figs. 2A and 4B). Theoretically, both the helical and sinusoidal waves can generate overlapping arrays of incoming flagella, which would promote continuous sperm cooperation. Another consideration for sperm to effectively enter tubular structures would be whether sperm have sufficient penetrating force to overcome resistance within the lumen. Like an Archimedes Screw, the corkscrew-like motion of helical waves is expected to have great penetrating force, and it likely displaces fluid in the opposite direction of the sperm's progressive movement, thereby displacing fluid out of the dead-ended SR tubule as the sperm enter it. The arc-line waveform would not be as

effective, because it simply stirs the fluid in all directions. However, fluid displacement usually does not occur in an environment with a high Reynolds number, and whether fluid displacement occurs during sperm entry into the PSR tubule requires further testing. Considering the need for rapidly advancing movement and continuous overlapping of sperm for cooperative movement, the sinusoidal or helical waveform would be a reasonable choice for sperm traveling into or out of narrow tubular structures.

Regulation of Bidirectional Movements

Drosophila sperm exhibit both tail-leading and head-leading movements. In sperm with shorter flagella, a common strategy for altering movement direction is by switching from symmetrical to asymmetrical bending waves. However, this strategy likely would not be effective for long sperm within the confines of the female SR, because the narrow lumen limits asymmetrical waves to mere micrometers on a millimeter-long sperm. By moving in both longitudinal directions, sperm have an alternative strategy for backing up or avoiding an obstacle via to-and-fro movement, as shown by sperm in the DSR (Supplemental Movie 10). Additional studies are needed to determine whether long sperm in insect species other than *D. melanogaster* also show bidirectional motility.

We showed that in flagellar waves associated with the arc-line waveform, movement initiates at the tail end, and sperm predominantly drag their heads behind the flagella in the uterus and DSR. In contrast, sperm leaving the storage tubules show predominantly head-leading movement. This suggests that a directional switch of flagellar waves takes place after sperm reside in the DSR. Such a switch could be important, because the next and most important task for sperm is to fertilize the egg. A *Drosophila* sperm enters the egg through a small micropyle canal on the anterior-most region of the egg shell [63]. Many *Drosophila* species have long sperm; while the head enters the egg, the tail tip hangs outside of the egg shell in at least four species analyzed, including *D. melanogaster,* which we study [64]. As the egg descends from the ovary, the micropyle of the egg faces the ventral SR opening on the oviduct [65]. A head-leading SR-exit orientation readies the sperm to enter the micropyle more quickly than a tail-leading orientation could. For this reason, the head-leading SR-exit orientation could be a physiological adaptation of sperm for efficient fertilization of the egg.

A Working Model for Sperm Storage

To begin PSR entry, a small number of sperm leave a selective, circular sperm focus in the uterus by forming a tail-leading, parallel bundle (Fig. 8, lane 1). As the tail-leading bundle moves forward into the PSR, additional sperm join in at the lagging end (Fig. 8, lane 2). In this manner, the entering sperm pass through the PSR as a continuous, overlapping, parallel array by drawing more and more sperm from the uterus. The assembly of new sperm into the moving sperm bundle is depicted by upward-moving sperm heads on the trail (Fig. 8, lane 3). Formation of the parallel sperm bundle is supported by observation of the GFP trail in the uterus (Fig. 3H and Supplemental Movie 9), the stalled tail bundle in the PSR (Fig. 3A and Supplemental Movie 6), and still images of intertwined sperm bundles in the PSR lumen (Figs. 2A and 4B). In addition, spacing between two adjacent moving sperm heads in video recordings of PSR-passing sperm, at both the early (Supplemental Movie 9) and later sperm storage periods (Supplemental Movies 7 and 8), is typically less than 2 mm, the full length of sperm (Supplemental Table S1). These results show that the sperm predominantly pass through the PSR in overlapping, parallel arrays.

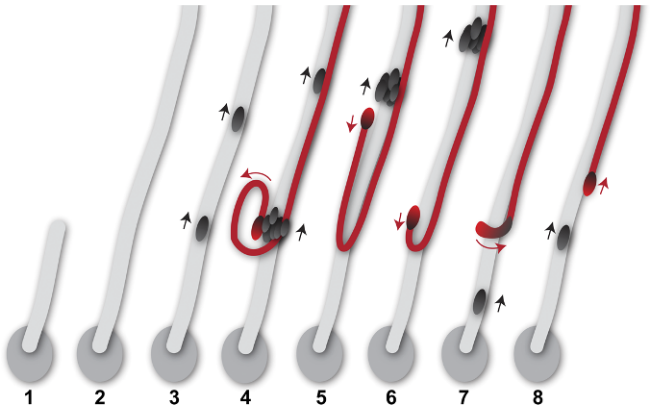

FIG. 8. A working model for PSR entry. Key events are shown in sequence. 1) Sperm move in circular foci in the uterus. One of the foci is depicted as an oval, representing the focus that has responded to the PSR entry signal. From this, sperm begin to form a parallel array with tails leading (gray stripe). 2) The sperm in the parallel array move into the PSR lumen on the top beyond our view, leading to the appearance of a GFP trail in Supplemental Movie 9. 3) As the sperm bundle moves upward, additional sperm are added from the circular focus, and the heads of these sperm appear on the trail at different times and move upward. This represents the behavior of most sperm entering the PSR (black heads). 4) A cluster of sperm heads, including one misaligned atypical head (red), appears on the trail and moves upward. 5 and 6) The atypical head is recognized by its subsequent separation from the head cluster and movement in an opposite direction (red arrow) with respect to the majority of sperm on the trail. If the situation depicted in 5 occurs within the PSR lumen, it would give rise to one head plus one flagellar loop in the mix of a tail bundle, as shown in Figure 2A. 6) As the tail of the atypical sperm continues to move upward, the head makes a U-turn and subsequently moves upward, just like the majority of sperm on the trail.

The parallel flagellar formation is preceded by folded sperm in the uterus, suggesting that PSR entry involves a waveform conversion, possibly triggered by a physiological PSR entry signal. To initiate waveform conversion, a folded flagellum, typically containing 10 arc-line bends, is gradually transformed into a linear form. The tail ends of the sperm would align into a parallel bundle first. As the tail ends straighten, the rest of the flagella would gradually straighten, and finally, the head ends would straighten. A few partially folded flagella could be incorporated into the moving sperm bundle before it is completely straightened. This would result in a few atypical sperm (Fig. 8, lane 4, red) with folded flagella and heads pointing in the wrong direction with respect to most sperm in the bundle (Fig. 8, lanes 4–6). As the tail of the atypical sperm moves upward on the trail, the atypical head moves in the opposite direction (Fig. 8, lanes 5 and 6). This atypical sperm would finally straighten out its U-shaped fold when the head undergoes a 180° turn (Fig. 8, lane 8). The behavior of the atypical sperm described here is visible in the upper portion of Supplemental Movie 9 when it is played at slow speed (see also Fig. 3).

A general phenomenon related to sperm in chemotactic settings is that only a small fraction (usually $<10\%$) respond chemotactically to physiological secretions (for review, see [1, 19]). Here, approximately 400 of roughly 5000 sperm in the uterus enter the PSR [52]. As the responding sperm form a parallel bundle, the adjacent nonresponding or partially responding sperm (e.g., the tail end responded, but the head end had not yet responded) might get carried into the sperm

bundle assembly with folded flagella. This could explain the preferential associations of atypical sperm with thick tail bundles (Figs. 2A and 4) or with large head clusters (Supplemental Movie 9). Alternatively, we cannot rule out that some small fraction of sperm might normally pass through the PSR in a folded form or a head-leading orientation. Heterogeneous sperm motility is known to occur in species that produce dimorphic sperm [50, 51]. However, *Drosophila* sperm appear to have a homogenous morphology. At this time, it is difficult to envision the possible advantages of having a low percentage of folded or head-leading sperm moving together with overlapping, parallel sperm arrays.

The Role of Pkd2 in Sperm Storage

The complexity of motility changes observed in the female reproductive tract suggests that many regulatory mechanisms are involved. We have shown that the Pkd2 calcium channel [66] regulates sperm entry movement into the SR. The success of this predominantly tail-leading movement is expected to require waveform conversion, maintenance of the appropriate waveform for PSR entry, and persistent wave propagation from the tail end. The role of Pkd2 in this process was shown by the mutant phenotypes. Without wild-type *Pkd2* activity, the mutant sperm entered the PSR with a wrong or random orientation and tended to form abnormal flagellar folds that impeded further movement into the storage site. The abnormal flagellar folds were likely generated by abnormal waveforms (i.e., abnormal flagellar propulsion) rather than by multiple turning movements of sperm with normal motility (Supplemental Movie 12). Thus, the mutant phenotypes revealed two defects—namely, waveform and wave propagation direction, both of which result from the temporal and spatial pattern of dynein motor activity on the axoneme. Waveform conversion and regulation of wave propagation could be two aspects of a single process that is regulated by Pkd2. The Pkd2-mediated process by which the sperm enter the SR shows some resemblance to the mating process of *Chlamydomonas reinhardtii*, in which the flagella of two opposite mating cell types twist around each other into a parallel bundle via agglutinin molecules on the flagellar surface and the PKD2 ion channel on the flagellum is required for signal transduction and completion of mating [67].

ACKNOWLEDGMENTS

We thank B.T. Wakimoto and R. Renkawitz-Pohl for sperm GFP reporters; Bloomington *Drosophila* Stock Center for fly stocks; R. Patten and R. Lillich for assistance with the Nikon microscope; D. Neumann for video processing; C.J. Brokaw, E.L. Ruden, and C.B. Lindemann for invaluable discussion; and D.M. Ruden for manuscript reading.

REFERENCES

1. Eisenbach M, Giojalas LC. Sperm guidance in mammals—an unpaved road to the egg. Nat Rev Mol Cell Biol 2006; 7:276–285.
2. Suarez SS. Regulation of sperm storage and movement in the mammalian oviduct. Int J Dev Biol 2008; 52:455–462.
3. Cho C, Bunch DO, Faure JE, Goulding EH, Eddy EM, Primakoff P, Myles DG. Fertilization defects in sperm from mice lacking fertilin beta. Science 1998; 281:1857–1859.
4. Ikawa M, Nakanishi T, Yamada S, Wada I, Kominami K, Tanaka H, Nozaki M, Nishimune Y, Okabe M. Calmegin is required for fertilin alpha/beta heterodimerization and sperm fertility. Dev Biol 2001; 240: 254–261.
5. Hagaman JR, Moyer JS, Bachman ES, Sibony M, Magyar PL, Welch JE, Smithies O, Krege JH, O'Brien DA. Angiotensin-converting enzyme and male fertility. Proc Natl Acad Sci U S A 1998; 95:2552–2557.
6. Krege JH, John SW, Langenbach LL, Hodgin JB, Hagaman JR, Bachman ES, Jennette JC, O'Brien DA, Smithies O. Male-female differences in fertility and blood pressure in ACE-deficient mice. Nature 1995; 375:146–148.
7. Birkhead TR. Sexual selection and the temporal separation of reproductive events: sperm storage data from reptiles, birds and mammals. Biol J Linnean Soc 1993; 50:295–311.
8. Harper MJ. Relationship between sperm transport and penetration of eggs in the rabbit oviduct. Biol Reprod 1973; 8:441–450.
9. Hunter RH, Nichol R. Transport of spermatozoa in the sheep oviduct: preovulatory sequestering of cells in the caudal isthmus. J Exp Zool 1983; 228:121–128.
10. Suarez SS. Sperm transport and motility in the mouse oviduct: observations in situ. Biol Reprod 1987; 36:203–210.
11. Gwathmey TM, Ignotz GG, Suarez SS. PDC-109 (BSP-A1/A2) promotes bull sperm binding to oviductal epithelium in vitro and may be involved in forming the oviductal sperm reservoir. Biol Reprod 2003; 69:809–815.
12. Ignotz GG, Lo MC, Perez CL, Gwathmey TM, Suarez SS. Characterization of a fucose-binding protein from bull sperm and seminal plasma that may be responsible for formation of the oviductal sperm reservoir. Biol Reprod 2001; 64:1806–1811.
13. Gwathmey TM, Ignotz GG, Mueller JL, Manjunath P, Suarez SS. Bovine seminal plasma proteins PDC-109, BSP-A3, and BSP-30-kDa share functional roles in storing sperm in the oviduct. Biol Reprod 2006; 75: 501–507.
14. Ignotz GG, Cho MY, Suarez SS. Annexins are candidate oviductal receptors for bovine sperm surface proteins and thus may serve to hold bovine sperm in the oviductal reservoir. Biol Reprod 2007; 77:906–913.
15. Hunter RH. Sperm transport and reservoirs in the pig oviduct in relation to the time of ovulation. J Reprod Fertil 1981; 63:109–117.
16. Overstreet JW, Cooper GW. Effect of ovulation and sperm motility on the migration of rabbit spermatozoa to the site of fertilization. J Reprod Fertil 1979; 55:53–59.
17. Suarez SS, Ho HC. Hyperactivated motility in sperm. Reprod Domest Anim 2003; 38:119–124.
18. Suarez SS, Osman RA. Initiation of hyperactivated flagellar bending in mouse sperm within the female reproductive tract. Biol Reprod 1987; 36: 1191–1198.
19. Kaupp UB, Kashikar ND, Weyand I. Mechanisms of sperm chemotaxis. Annu Rev Physiol 2008; 70:93–117.
20. Spehr M, Gisselmann G, Poplawski A, Riffell JA, Wetzel CH, Zimmer RK, Hatt H. Identification of a testicular odorant receptor mediating human sperm chemotaxis. Science 2003; 299:2054–2058.
21. Hunter RH. Polyspermic fertilization in pigs after tubal deposition of excessive numbers of spermatozoa. J Exp Zool 1973; 183:57–63.
22. Woolley DM. Flagellar oscillation: a commentary on proposed mechanisms. Biol Rev Camb Philos Soc 2010; 85:453–470.
23. Brokaw CJ. Thinking about flagellar oscillation. Cell Motil Cytoskeleton 2009; 66:425–436.
24. Gibbons IR. Cilia and flagella of eukaryotes. J Cell Biol 1981; 91:107S–124S.
25. Holwill ME, Satir P. A physical model of microtubule sliding in ciliary axonemes. Biophys J 1990; 58:905–917.
26. Woolley DM, Vernon GG. A study of helical and planar waves on sea urchin sperm flagella, with a theory of how they are generated. J Exp Biol 2001; 204:1333–1345.
27. Woolley DM. A novel motility pattern in quail spermatozoa with implications for the mechanism of flagellar beating. Biol Cell 2007; 99: 663–675.
28. Bayly PV, Lewis BL, Kemp PS, Pless RB, Dutcher SK. Efficient spatiotemporal analysis of the flagellar waveform of *Chlamydomonas reinhardtii*. Cytoskeleton (Hoboken) 2010; 67:56–69.
29. Brokaw CJ. Effects of increased viscosity on the movements of some invertebtate spermatozoa. J Exp Biol 1966; 45:113–139.
30. Satir P. Switching mechanisms in the control of ciliary motility. Mod Cell Biol 1985; 4:1–46.
31. Satir P, Matsuoka T. Splitting the ciliary axoneme: implications for a ''switch-point'' model of dynein arm activity in ciliary motion. Cell Motil Cytoskeleton 1989; 14:345–358.
32. Morita Y, Shingyoji C. Effects of imposed bending on microtubule sliding in sperm flagella. Curr Biol 2004; 14:2113–2118.
33. Brokaw CJ. Computer simulation of flagellar movement. VIII: coordination of dynein by local curvature control can generate helical bending waves. Cell Motil Cytoskeleton 2002; 53:103–124.
34. Ishijima S, Ishijima SA, Afzelius BA. Movement of *Myzostomum* spermatozoa: calcium ion regulation of swimming direction. Cell Motil Cytoskeleton 1994; 28:135–142.
35. Ishijima S, Ishijima SA, Afzelius BA. Movement of *Turritella*

spermatozoa: direction of propagation and chirality of flagellar bends. Cell Motil Cytoskeleton 1999; 44:85–95.
36. Baccetti B, Gibbons BH, Gibbons IR. Bidirectional swimming in spermatozoa of Tephritid flies. J Submicrosc Cytol Pathol 1989; 21: 619–625.
37. Rathke C, Baarends WM, Jayaramaiah-Raja S, Bartkuhn M, Renkawitz R, Renkawitz-Pohl R. Transition from a nucleosome-based to a protamine-based chromatin configuration during spermiogenesis in *Drosophila*. J Cell Sci 2007; 120:1689–1700.
38. Santel A, Winhauer T, Blumer N, Renkawitz-Pohl R. The *Drosophila* don juan (dj) gene encodes a novel sperm specific protein component characterized by an unusual domain of a repetitive amino acid motif. Mech Dev 1997; 64:19–30.
39. Gao Z, Ruden DM, Lu X. PKD2 cation channel is required for directional sperm movement and male fertility. Curr Biol 2003; 13:2175–2178.
40. Watnick TJ, Jin Y, Matunis E, Kernan MJ, Montell C. A flagellar polycystin-2 homolog required for male fertility in *Drosophila*. Curr Biol 2003; 13:2179–2184.
41. Walker PJ. Organization of function in trypanosome flagella. Nature 1961; 189:1017–1018.
42. Sugrue P, Hirons MR, Adam JU, Holwill ME. Flagellar wave reversal in the kinetoplastid flagellate *Crithidia oncopelti*. Biol Cell 1988; 63:127–131.
43. Lindemann CB. The geometric clutch as a working hypothesis for future research on cilia and flagella. Ann N Y Acad Sci 2007; 1101:477–493.
44. Woolley D, Gadelha C, Gull K. Evidence for a sliding-resistance at the tip of the trypanosome flagellum. Cell Motil Cytoskeleton 2006; 63:741–746.
45. Fujimura M, Okuno M. Requirement of the fixed end for spontaneous beating in flagella. J Exp Biol 2006; 209:1336–1343.
46. Woolley DM, Bozkurt HH. The distal sperm flagellum: its potential for motility after separation from the basal structures. J Exp Biol 1995; 198: 1469–1481.
47. Goldstein SF. Irradiation of sperm tails by laser microbeam. J Exp Biol 1969; 51:431–441.
48. Okuno M, Hiramoto Y. Mechanical stimulation of starfish sperm flagella. J Exp Biol 1976; 65:401–413.
49. Goldstein SF, Holwill ME, Silvester NR. The effects of laser microbeam irradiation on the flagellum of *Crithidia* (*Strigomonas*) *oncopelti*. J Exp Biol 1970; 53:401–409.
50. Moore H, Dvorakova K, Jenkins N, Breed W. Exceptional sperm cooperation in the wood mouse. Nature 2002; 418:174–177.
51. Immler S. Sperm competition and sperm cooperation: the potential role of diploid and haploid expression. Reproduction 2008; 135:275–283.
52. Manier MK, Belote JM, Berben KS, Novikov D, Stuart WT, Pitnick S. Resolving mechanisms of competitive fertilization success in *Drosophila melanogaster*. Science 2010; 328:354–357.
53. Bloch Qazi MC, Wolfner MF. Emergence of sperm from female storage sites has egg-influenced and egg-independent phases in *Drosophila melanogaster*. Biol Lett 2006; 2:128–130.
54. Neubaum DM, Wolfner MF. Wise, winsome, or weird? Mechanisms of sperm storage in female animals. Curr Top Dev Biol 1999; 41:67–97.
55. Rodriguez JA, Lopez MA, Thayer MC, Zhao Y, Oberholzer M, Chang DD, Kisalu NK, Penichet ML, Helguera G, Bruinsma R, Hill KL, Miao J. Propulsion of African trypanosomes is driven by bihelical waves with alternating chirality separated by kinks. Proc Natl Acad Sci U S A 2009; 106:19322–19327.
56. Rice WR. Sexually antagonistic male adaptation triggered by experimental arrest of female evolution. Nature 1996; 381:232–234.
57. Gavrilets S. Rapid evolution of reproductive barriers driven by sexual conflict. Nature 2000; 403:886–889.
58. Pitnick S, Markow T, Spicer GS. Evolution of multiple kinds of female sperm-storage organs in *Drosophila*. Evolution 1999; 53:1804–1822.
59. Miller GT, Pitnick S. Functional significance of seminal receptacle length in *Drosophila melanogaster*. J Evol Biol 2003; 16:114–126.
60. Presgraves DC, Baker RH, Wilkinson GS. Coevolution of sperm and female reproductive tract morphology in stalk-eyed flies. Proc R Soc Lond B Biol Sci 1999; 268:1041–1047.
61. Miller GT, Pitnick S. Sperm-female coevolution in *Drosophila*. Science 2002; 298:1230–1233.
62. Pitnick S, Miller GT, Schneider K, Markow TA. Ejaculate-female coevolution in *Drosophila mojavensis*. Proc Biol Sci 2003; 270:1507–1512.
63. Montell DJ, Rorth P, Spradling AC. Slow border cells, a locus required for a developmentally regulated cell migration during oogenesis, encodes *Drosophila* C/EBP. Cell 1992; 71:51–62.
64. Karr TL, Pitnick S. The ins and outs of fertilization. Nature 1996; 379: 405–406.
65. Snook RR, Karr TL. Only long sperm are fertilization-competent in six sperm-heteromorphic *Drosophila* species. Curr Biol 1998; 8:291–294.
66. Venglarik CJ, Gao Z, Lu X. Evolutionary conservation of *Drosophila* polycystin-2 as a calcium-activated cation channel. J Am Soc Nephrol 2004; 15:1168–1177.
67. Huang K, Diener DR, Mitchell A, Pazour GJ, Witman GB, Rosenbaum JL. Function and dynamics of PKD2 in *Chlamydomonas reinhardtii* flagella. J Cell Biol 2007; 179:501–514.